Supporting Appendix for:

Molecular bases for the selection of the chromophore of animal rhodopsins

Hoi Ling Luk, Federico Melaccio, Silvia Rinaldi, Samer Gozem, Massimo Olivucci

Department of Chemistry, Bowling Green State University, Bowling Green OH 43403, USA
Dipartimento di Biotecnologie, Chimica e Farmacia, Università di Siena, Siena, I-53100, Italy

1. QM/MM models

1.1 Model Construction

Here we report on the detailed workflow for the construction of the selected (reference) quantum mechanics/molecular mechanics (QM/MM) models of the two Anabaena Sensory Rhodopsin forms with the 13-*cis* chromophore (ASR_{13C}) and all-*trans* chromophore (ASR_{AT}) discussed in the main text. Our target is to construct QM/MM models that can reproduce all the relevant observed static and transient spectroscopic data so that they can be employed to study the molecular mechanisms presented in the main text. The corresponding and consistent QM/MM Rh model employed in this work has been recently reported (1) and its construction is therefore not detailed here.

The ASR models were prepared using the available 2.0 Å resolution crystallographic structures (PDB code: 1XIO) (2) which show a mixture of the 13-*cis* and all-*trans* chromophores. Membrane lipids at the protein surface were excluded in the model while all the crystallographic water molecules were maintained. In order to have a neutral system overall, we set the total charge on the protein (MM subsystem) to -1 (the QM subsystem, which contains the chromophore bears a +1 charge due to protonated Schiff base linkage). Accordingly a number of chloride ions were added near positively charged residues (such as Arg, His) on the protein surface and far away from the chromophore. The positions of chloride ions were found to have a limited effect on the spectroscopic properties of the chromophore, as well as on test trajectories. Amino acid ionization states were determined with PROPKA 3.0. (3, 4) For Rh, we use a protonated form of E181. There are several conflicting experimental and computational conflicting studies on the protonation state of E181 (5-10). In our own model, deprotonation of E181 leads to a ~60 nm blue-shift of the computed absorption maxima indicating an unbalanced/incorrect electrostatic environment around the chromophore. This is consistent with other QM/MM reports where it was reported that deprotonation of the E181 leads to a large blue-shift (see the supporting information of (9) and also (8) and (10).

The retinal chromophore was treated quantum mechanically using the *ab initio* complete-active-space self consistent field (CASSCF) method. (11) The protein environment is described by the AMBER94 force field (12) with modified parameters for the Lys residue linked to the chromophore. (13, 14) Electrostatic embedding was used to describe the interaction between the MM and QM subsystems using the ESPF concept. (15-17) CASSCF is a flexible multiconfigurational method for an unbiased description of the electronic character on both excited and ground state (i.e. with no empirical derived parameters and avoiding single-reference wavefunctions). Equilibrium and transition state structures were optimized at the single-root CASSCF(12,12)/6-31G*/AMBER level. QM/MM calculations were carried out with Molcas 7.8 (18) and Tinker 5.1 (19) programs, within the microiterations approach. (17) The QM/MM boundary is at the Lys Cδ-Cε bond and the link-atom scheme was used to treat the frontier between the QM and MM subsystems. (20) The partitioning of QM and MM atoms was as follows:

- QM atoms: all retinal atoms, five atoms of the lysine chain connected to it (ε-nitrogen, ε-carbon and their hydrogen atoms and the link atom. There are 54 QM atoms in total.
- Explicit MM atoms: the remaining 9 atoms of the lysine side-chain are treated explicitly by Molcas (as opposed to other atoms which are treated by Tinker). These atoms are optimized along with the QM part and not by microiterations as the other MM atoms (see below).
- ACTIVE MM atoms: for ASR_{13C} and ASR_{AT} these are given by the union set of all the side-chains or waters that has at least one atom that is within 4 Å from the QM region. These MM atoms are optimized using the microiteration methods available in Molcas/Tinker.
- INACTIVE MM atoms: all the remaining atoms. These atoms contribute to the electrostatic environment around the chromophore but their geometries are kept frozen during QM/MM optimizations.

Here, we provide the general protocol used to construct our QM/MM models starting from the crystal structure:

- Addition of the hydrogens to crystallographic waters and the side chain polar atoms using DOWSER (21);
- Addition of the remaining hydrogen atoms using pdb2gmx command in GROMACS (22);
- MM minimization of all hydrogen atoms, keeping heavier atoms fixed in their original crystallographic positions.
- Simulated annealing on all hydrogen atoms is performed by heating up to 600 K in 100 ps and then cooling down to 0 K in 500 ps.
- The final structure is used to perform molecular dynamics on any amino acid side chain featuring at least one atom within 6 Å from any retinal chromophore atom at 298 K. The last snapshot of the molecular dynamics was used to perform a MM minimization on all hydrogen atoms.
- A QM/MM Hartree-Fock/3-21G single point calculation was performed to calculate ESPF charges on QM atoms;
- Tinker minimization of ACTIVE MM atoms using the calculated ESPF charges, with the same settings used for hydrogen atoms minimization;
- QM/MM Molcas/Tinker HF/3-21G optimization of the system with ACTIVE atoms relaxed;
- QM/MM Molcas/Tinker CASSCF(12,12)/3-21G optimization of the system with ACTIVE atoms relaxed;
- QM/MM Molcas/Tinker CASSCF(12,12)/6-31G* optimization of the system with ACTIVE atoms relaxed.

The CASSCF geometries were used for subsequent multiconfigurational second-order perturbation theory (CASPT2) single point energy computations (23) that allow for a more quantitative evaluation of the excitation energies and excited state energy differences by accounting for the dynamic electron correlation (XMCQDPT2 energy corrections have also been used instead of CASPT2, see details in Section 4). The CASPT2 energies were computed with an imaginary shift of 0.2 to exclude possible intruder states, and with the IPEA shift (24) set to zero thus overriding the default value of 0.25. It has been shown that the CASPT2(IPEA=0)//CASSCF/6-31G* protocol (the double slash // indicates single-point calculations with the level used for geometry optimization indicated after it) yields excitation energies in better agreement with MRCISD+Q//CASPT2(IPEA=0.25)/ANO-L-VTZP reference computations than CASPT2(IPEA=0.25)//CASSCF/6-31G*, for a small model of the 11-*cis* retinal protonated Schiff base (PSB11) chromophore featuring three conjugated double bonds (PSB3). (25) This is due to a cancellation of errors which originates from opposite energy differences due to the geometries, correlation energies (i.e. method and IPEA correction) and basis sets with respect to the reference. (25) Since systematic CASPT2 minima and transition state geometry optimizations as well as trajectory computations (e.g. intercepting potential energy crossings) are currently unfeasible for a chromophore such as PSB11 (i.e. one is forced to use a CASSCF level), we used the CASPT2(IPEA=0)//CASSCF/6-31G*/AMBER protocol. This appears to be, presently, a viable compromise if equilibrium structures, excitation energies, trajectories, conical intersections and transition states with different electronic structures need to be computed on a common methodological basis and if the main focus is on mechanistic studies rather than quantitative studies. The final geometry optimization leads to a CASSCF(12,12)/6-31G*/AMBER equilibrium structure for all ASR models.

1.2 Trajectory Computations

Excited state (S_1) trajectories were calculated using the Molcas module Dynamix which is described in more detail in ref. (26). The trajectories were calculated at the two-root state-averaged CASSCF/6-31G*/AMBER level followed by three-root state-averaged CASPT2 (or XMCQPT2, see detail in Section 4) corrections (also used to scale the CASSCF energy profiles). Since we are only interested in the evolution on S_1 from the Frank-Condon (FC) to the CI region, all trajectories were propagated until entering the region of a S_1/S_0 CI, according to the energy and wavefunction criteria implemented in Dynamix, (26) or until reaching a 200 fs time threshold. The ultrafast lifetime of these processes should ensure that a Franck-Condon trajectory (i.e. a trajectory starting from the Franck-Condon point with zero initial velocities) describes the average evolution of the corresponding S_1 population as discussed in the main text.

Trajectory calculations were always performed using two, rather than three, state-avereaged roots as best compromise for the quality of the S_1 CASSCF wavefunction. (25) In fact, while the S_1 state is dominated by a charge-transfer character and S_0 has a covalent (closed shell) character, the third root has a covalent (diradical) character. We found (25) that the three-root wave function has a far too high covalent character. This may lead to an S_1 gradient which may significantly deviate from the correct one as the system progress towards the S_1/S_0 (or S_2/S_1) conical intersections. Hence, all trajectories were performed at two state-averaged roots to maintain a more balanced description of the charge transfer and covalent character in the S_1 wavefunction. Of course, to account for the effect of the S_2 state on the energy profiles correctly, we went beyond the CASSCF representation and corrected the energy profiles and oscillator strengths at the CASPT2 and also XMCQPT2 levels using, as zeroth order wavefunctions, three state-averaged CASSCF wavefunctions. Tests for the effect of the state-averaging with three and four roots were performed and shown in Section 8.

1.3 Assignment of the Initial Lys210 Conformation

The x-ray crystallographic structure (2) is measured as a mixture of two conformations (A and B in Table S1) which may or may not be not associated in a one-to-one correspondence with the all-*trans* (AT) and 13-*cis* (13C) stereoisomer of the chromophore in the ASR_{AT} and ASR_{13C} respectively. In conformation A, the Lys210 side chain features all *anti* dihedrals along the entire carbon chain with only one *syn* dihedral for angle Cγ-Cδ-Cε-N. In contrast, in the conformer B, the Lys210 side chain has all *anti* dihedrals along the carbon chain except for angle Cα-Cβ-Cγ-Cδ which is *syn*. Hence, for both the 13C and AT chromophore, there are two possible side chain choices as shown in Fig. S1 (Model I (27) and Model II (2)). Both models are found to be acceptable in terms of the omit map which is displayed in Fig. S1C for Model I. However, Model I is the model ultimately employed for our research and the only one considered in the main text. In the following we discuss this selection.

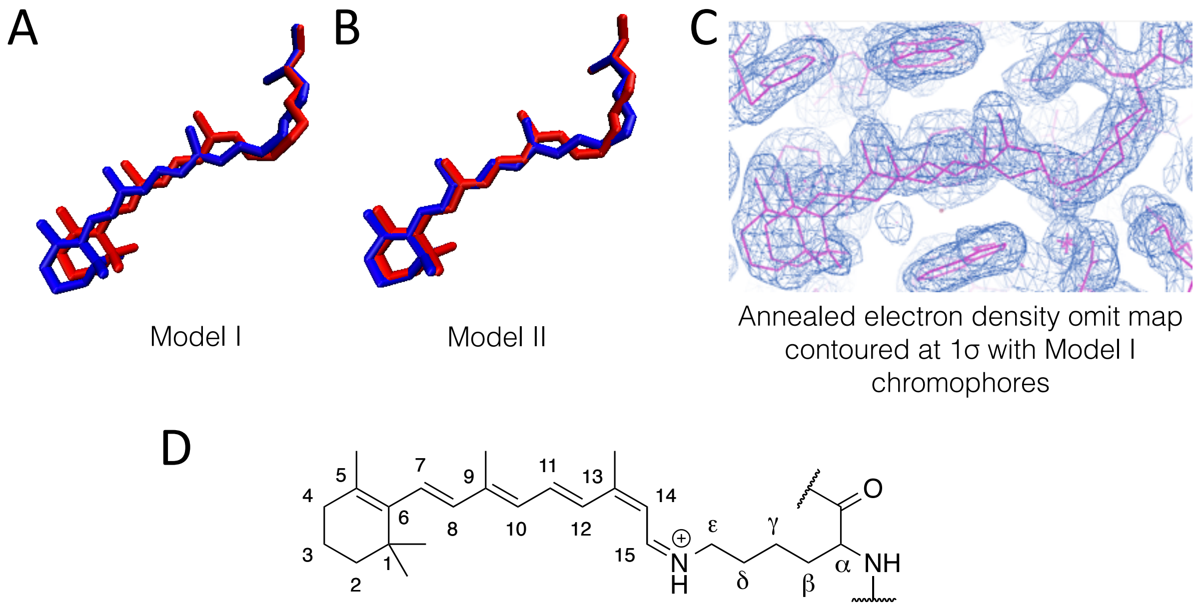

Fig. S1. Possible Lys210 conformations for ASR_{13C} and ASR_{AT} in (A) Model I and (B) Model II (see Table S1 for details). Geometries of ASR_{13C} (red) and ASR_{AT} (blue) with the corresponding lysine chain. (C) Annealed electron density omit map contoured at 1σ with Model I chromophores (D) Scheme showing atom labels on the retinal chromophore and Lys210 chain.

Table S1. Possible combinations of retinal-bound lysine (Lys210) conformations

Models	Chromophore configuration	Lysine	Cγ-Cδ-Cε-N	Cα-Cβ-Cγ-Cδ
Model I	ASR_{AT}	B	anti	syn
	ASR_{13C}	A	syn	anti
Model II	ASR_{AT}	A	syn	anti
	ASR_{13C}	B	anti	syn

Both Model I and Model II are capable to reproduce the vertical excitation energies ($\Delta E_{S1\text{-}S0}$) associated with the observed absorption maxima (λ_{max}) within 3 kcal mol^{-1} (Table S2). however, it is found that when using Model II the S_1/S_0 conical intersection is never reached within 200 fs in contrast with time resolved spectral data in which ASR_{13C} would decay in less than 150 fs and much faster than ASR_{AT}. (28) This suggests that Model II is not suitable for mechanistic investigations. In contrast, Model I shows qualitative consistency with the transient spectral data. (28) Furthermore, we showed (see text) that Model I yields consistent values for the observed fluorescence emission (29) and K photocycle intermediate absorption (30). For Model I both the CASSCF/3-21G and CASSCF/6-31G* trajectories showed similar energy profiles (Fig. S2A). Given the similarity in the energy profiles Model II was investigated using the smaller (3-21G) basis set due to the more affordable computational cost.

Table S2. Computed and experimental vertical excitation energies and absorption maxima (λ_{max}) values.The λ_{max} values are given in brackets. Trajectory calculations were performed with CASSCF(12,12)/3-21G/AMBER.

	Model, $\Delta E_{S1\text{-}S0}$ kcal mol^{-1} (nm)	Observed, $\Delta E_{S1\text{-}S0}$ kcal mol^{-1} (nm)	Model, $\Delta E_{S2\text{-}S0}$ kcal mol^{-1} (nm)	Oscillator strength, $S_0 \rightarrow S_1$	Oscillator strength, $S_0 \rightarrow S_2$	Isolat. PSB, $\Delta E_{S1\text{-}S0}$ kcal mol^{-1} (nm)	Isolat. PSB, $\Delta E_{S2\text{-}S0}$ kcal mol^{-1} (nm)	Hop in 200fs?
ASR_{13C} (Model I)	54.2 (527)	53.2 (537)	79.4 (360)	0.9	0.4	46.6 (614)	74.5 (383)	Y
ASR_{AT} (Model I)	53.6 (533)	52.1 (549)	77.4 (369)	1.0	0.5	45.4 (629)	72.9 (392)	N
ASR_{13C} (Model II)	54.6 (522)	53.2 (537)	80.2 (356)	1.0	0.4	47.0 (608)	74.6 (383)	N
ASR_{AT} (Model II)	53.8 (531)	52.1 (549)	77.1 (370)	1.1	0.5	45.5 (628)	72.9 (392)	N

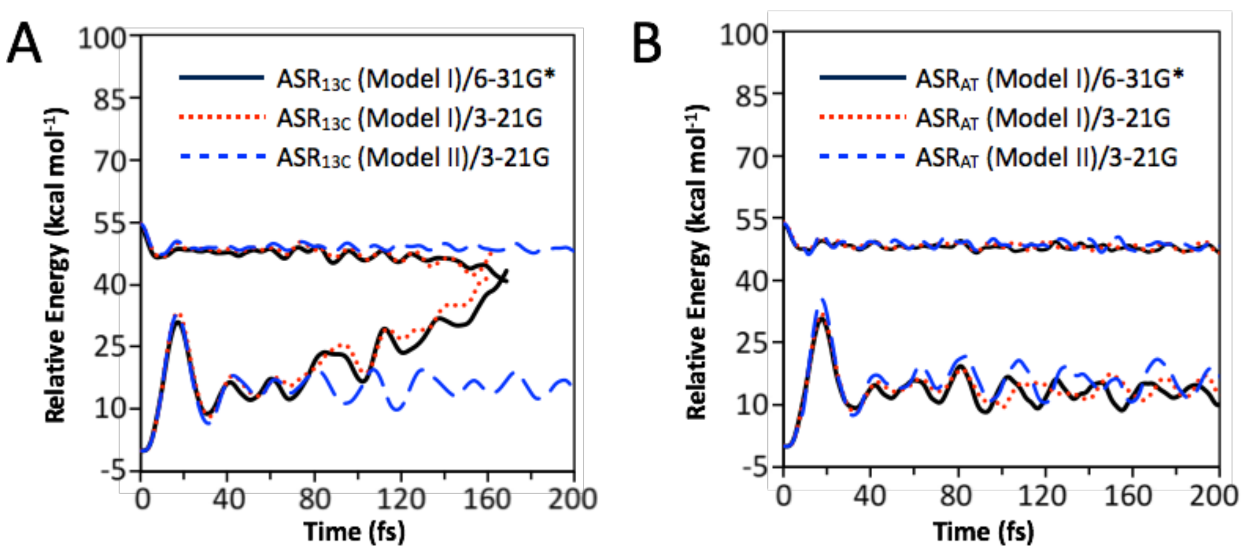

Fig. S2. QM/MM trajectory for (A) ASR_{13C} and (B) ASR_{AT} computed with scaled-CASSCF(12,12)/AMBER corrected at the CASPT2/6-31G* level of theory (31) based on different lysine conformations (Model I or Model II) as specified in Table S1.

2. Energies and structures.

2.1 Excitation energies and their analysis.

Table S3. Computed and experimental vertical excitation energies and absorption maxima (λ^{a}_{max}) values.

	Model, $\Delta E_{S1\text{-}S0}$ kcal mol^{-1} (nm)	Observed, $\Delta E_{S1\text{-}S0}$ kcal mol^{-1} (nm)	Model, $\Delta E_{S2\text{-}S0}$ kcal mol^{-1} (nm)	Model, $\Delta E_{S2\text{-}S1}$ kcal mol^{-1}	Oscillator strength, $S_0 \rightarrow S_1$	Oscillator strength, $S_0 \rightarrow S_2$	Isolat. PSB, $\Delta E_{S1\text{-}S0}$ kcal mol^{-1} (nm)	Isolat. PSB, $\Delta E_{S2\text{-}S0}$ kcal mol^{-1} (nm)	Isolat. PSB, $\Delta E_{S2\text{-}S1}$ kcal mol^{-1}
ASR_{AT}	53.6 (533)	52.1 (549)	77.4 (369)	23.8	1.0 (1.00)	0.5 (0.34)	45.4 (629)	72.9 (392)	27.5
ASR_{13C}	54.2 (527)	53.2 (537)	79.4 (360)	25.2	0.9 (0.89)	0.4 (0.25)	46.6 (614)	74.5 (383)	27.9
Rh	57.3 (499)	57.4 (498)	83.6 (342)	26.3	0.9 (0.83)	0.4 (0.25)	50.5 (566)	81.0 (353)	30.5

The λ^{a}_{max} values are given in parentheses. ASR_{13C}, and ASR_{AT}, *Anabaena* sensory rhododpsins; Rh, bovine rhodopsin. XMCQDPT2 (see text for the acronym definition) oscillator strengths are given in parentheses.

2.2 Effects of the Chromophore β-ionone Ring Twisting, Backbone Conjugation and Cis versus Trans configuration.

In order to determine the origin of the larger $\Delta E_{S2\text{-}S1}$ gap along the Rh trajectory compared to the ASR trajectories, we manually modified the C5-C6-C7-C8 dihedral angle of the Rh isolated chromophore (i.e. in the gas phase) to the 171º value (same as the corresponding dihedral in ASR_{13C}). Such a modified Rh structure gave a $\Delta E_{S2\text{-}S1}$ value of 25 kcal mol^{-1} which is sensibly smaller than in the original Rh chromophore isolated from the protein cavity (30.5 kcal mol^{-1}), indication that the gap between the S_2 and S_1 states is, at least in part, controlled by the value of the C5-C6-C7-C8 dihedral angle.

Table S4. CASPT2 S_1-S_0 and S_2-S_1 energy gaps (in kcal mol^{-1}) for structures optimized on the ground, first and second excited state while imposing C_s symmetry, for 3, 4, 5 and 6 double-bonded protonated Schiff base models.

		PSB6	PSB5	PSB4	PSB3
S_0-min	$\Delta E_{S1\text{-}S0}$	53.8	62.7	75.3	94.7
	$\Delta E_{S2\text{-}S1}$	21.7	23.4	26.2	30.4
S_1-min	$\Delta E_{S1\text{-}S0}$	41.7	49.5	60.3	76.4
	$\Delta E_{S2\text{-}S1}$	17.9	19.1	20.7	22.7
S_2-min	$\Delta E_{S1\text{-}S0}$	48.7	57.1	68.6	84.3
	$\Delta E_{S2\text{-}S1}$	5.0	6.2	8.0	12.0

The magnitude of the S_2-S_1 energy gap depends also on the number of double bonds in the system, as well as the values of the single and double bond lengths along the chromophore backbone since these modulate the π-bond conjugation. For this reason, we looked at the effect of the chromophore π-conjugation on the $\Delta E_{S2\text{-}S1}$ and $\Delta E_{S1\text{-}S0}$ values of different protonated Schiff base models (PSBn where n = 3, 4, 5 or 6 which corresponds to the number of double bonds) in isolated conditions (gas phase). These were optimized at CASSCF(2n,2n)/6-31G* level (where n corresponds to the number of double bonds) on each of the S_0, S_1 and S_2 states while imposing C_s symmetry. The optimization on different states yields geometries with different bond alternation (and π-conjugation) patterns (in S_1 the pattern is inverted with respect to S_0 while in S_2 the pattern is more an even one in which single and double bonds have closer lengths). The corresponding CASPT2 ΔE_{S1-S0} and ΔE_{S2-S1} values are reported in Table S4. These optimized structures show that both values increase when the length of chromophore conjugations decreases. (Table S4)

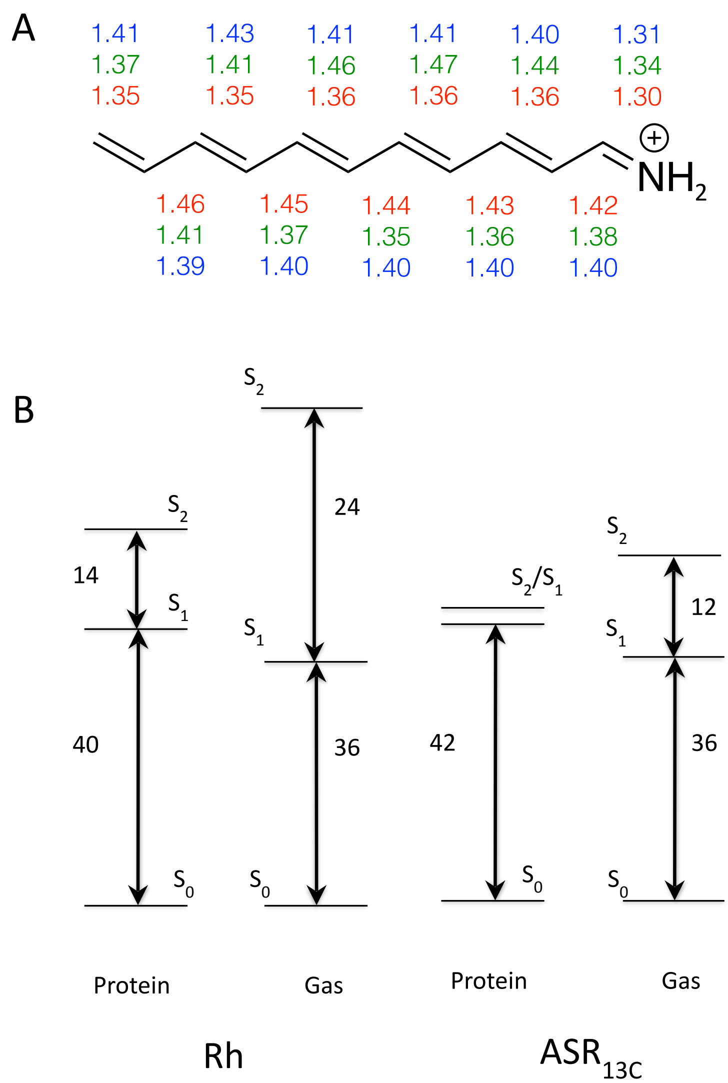

Fig. S6. (A) PSB6 geometries optimized at CASSCF(12,12)/6-31G* at S_0, S_1 and S_2 states with C_s symmetry. Bond lengths are given in Å for S_0 in red, S_1 in green and S_2 in blue (B) Single point CASPT2 calculations on two structures selected from Rh (left) and ASR_{13C} (right) trajectories in which shows a 14° twist of the corresponding isomerizing bond with respect to the equilibrium structures. The energy gaps between the lowest three states were calculated in both the presence and absence (gas) of the apoprotein. All CASPT2 energies are reported in kcal mol^{-1}.

Finally, the effect of the protein on the S_2/S_1 degeneracy region was investigated. We selected the point along the Rh trajectory that gives the smallest S_2-S_1 energy gap. Such point features a +14º twist about the chromophore 11-*cis* double bond with respect to the Rh S_0 equilibrium structure (at ca. 30 fs). Then, in order to maintain geometrical similarity, we selected the corresponding ASR_{13C} geometry with the same +14º twist (at ca. 40 fs) with respect to its S_0 equilibrium structure. Both of these structures have a similar BLA value (within 0.035 Angstroms of each other). Fig. S6 shows results from these snapshots with twisted C13=C14 and C11=C12 for ASR_{13C} and Rh respectively. Single point CASPT2 calculations were performed for the corresponding chromophore structures in both the presence and absence of the protein environment. These results show that even in the absence of the apoprotein, ASR_{13C} has a smaller S_2-S_1 gap with respect to Rh. As we have shown above, this is most likely due to a reduced conjugation in the Rh chromophore backbone partly due to the larger β-ionone ring twisting. In addition to the effect of the chromophore geometry, the protein environment is helping to further reduce the S_2-S_1 energy gap in ASR_{13C} by ca. 12 kcal mol^{-1}. This results in a S_2/S_1 degeneracy. In contrast, in the Rh case, the protein only reduces the S_2-S_1 gap by 10 kcal mol^{-1}, resulting in a structure where the ΔE_{S2-S1} value is 14 kcal mol^{-1}. Such analysis is not possible for ASR_{AT} as the C13=C14 bond twisting of ASR_{AT} remains within 10 degrees. We assume that the ASR_{13C} results can be safely extended to ASR_{AT}.

Notice that PSB11 in methanol solution only isomerizes about the C11=C12 bond while the PSBAT isomerizes at both the C11=C12, C9=C10 and in smaller percentage, C13=C14 bonds (32). However, this isomerization is much slower and has smaller quantum yields. More precisely, while the selection of PSB11 may have been based on its propensity for bond selective isomerization, the excited state lifetimes of both PSBAT (33) and PSB11 in solution (34) is much longer (few ps) than in the protein cavity (hundred of fs), the photoisomerization quantum yield is 20% in methanol solution but over 50% in the protein cavity (32). Therefore, the interaction with the protein cavity must have important effects.

3. Multiple Trajectory Testing and ASR Ground State Relaxation.

Table S5. Spectroscopic and photoreactivity properties computed on the basis of the QM/MM models derived after thermal sampling of the cavity residues of ASR_{13C} and ASR_{AT} models. The first 600 ps of the total 1.4 ns molecular dynamics run are used for snapshots. Note that the generated QM/MM models labels (700, 800 .. 1400) simply correspond to the time, in ps, at which the snapshot was selected from the MD simulation.

ASR_{13C}	Model, ΔE_{S1-S0} kcal mol^{-1} (nm)	Model, ΔE_{S2-S0} kcal mol^{-1} (nm)	Model, ΔE_{S2-S1} kcal mol^{-1} (nm)	S_2/S_1 degeneracy?	Hop Time (fs)
reference	54.2 (528)	79.4 (360)	25.2	Y	156
700	53.5 (535)	78.5 (364)	25.0	N	152
800	53.8 (532)	78.6 (364)	24.9	Y	144
900	53.6 (534)	78.6 (364)	25.1	Y	143
1000	53.4 (535)	78.6 (364)	25.1	Y	138
1100	53.6 (534)	78.6 (364)	25.0	Y	145
1200	53.6 (534)	78.4 (365)	24.9	Y	149
1300	53.5 (534)	78.5 (364)	25.0	Y	143
1400	53.7 (532)	78.5 (365)	24.7	N	184
Average	53.6 (533)	78.6 (364)	25.0		150 ± 14

ASR_{AT}	Model, ΔE_{S1-S0} kcal mol^{-1} (nm)	Model, ΔE_{S2-S0} kcal mol^{-1} (nm)	Model, ΔE_{S2-S1} kcal mol^{-1} (nm)	S_2/S_1 degeneracy?	Hop Time (fs)
reference	53.2 (537)	76.5 (374)	23.3	Y	> 200
700	53.2 (538)	76.5 (374)	23.4	Y	184
800	53.1 (538)	76.4 (375)	23.2	N	160
900	53.1 (539)	76.5 (374)	23.4	Y	> 200
1000	53.2 (537)	76.6 (373)	23.4	Y	> 200
1100	53.2 (538)	76.5 (374)	23.3	Y	> 200
1200	53.1 (538)	76.5 (374)	23.3	Y	> 200
1300	53.0 (539)	76.2 (375)	23.2	Y	> 200
1400	53.1 (539)	76.3 (375)	23.3	Y	> 200
Average	53.1 (539)	76.4 (375)	23.3		> 200

In order to assess the robustness of the documented S_2/S_1 degeneracy in ASR we used a sampling procedure to generate additional QM/MM model which were then used to run additional trajectories and check the stability of the behavior observed in our reference models. Accordingly, the reference ASR models have been used as starting geometries for a 1.4 ns molecular dynamics (MD) simulation at room temperature of the 4 Å chromophore cavity including waters and residues. Again, the scope is to test the models against a change of initial conditions after a short thermal sampling to further confirm the validity of our reference trajectory. During both the ASR_{13C} and ASR_{AT} dynamics the chromophore was frozen at its reference optimized geometry but could interact with the sampled waters and residues through its ESPF charges and van der Waals potentials. From such simulations, 8 snapshots were extracted and reoptimized at the QM/MM level, yielding a final set of 8 QM/MM models for each ASR form.

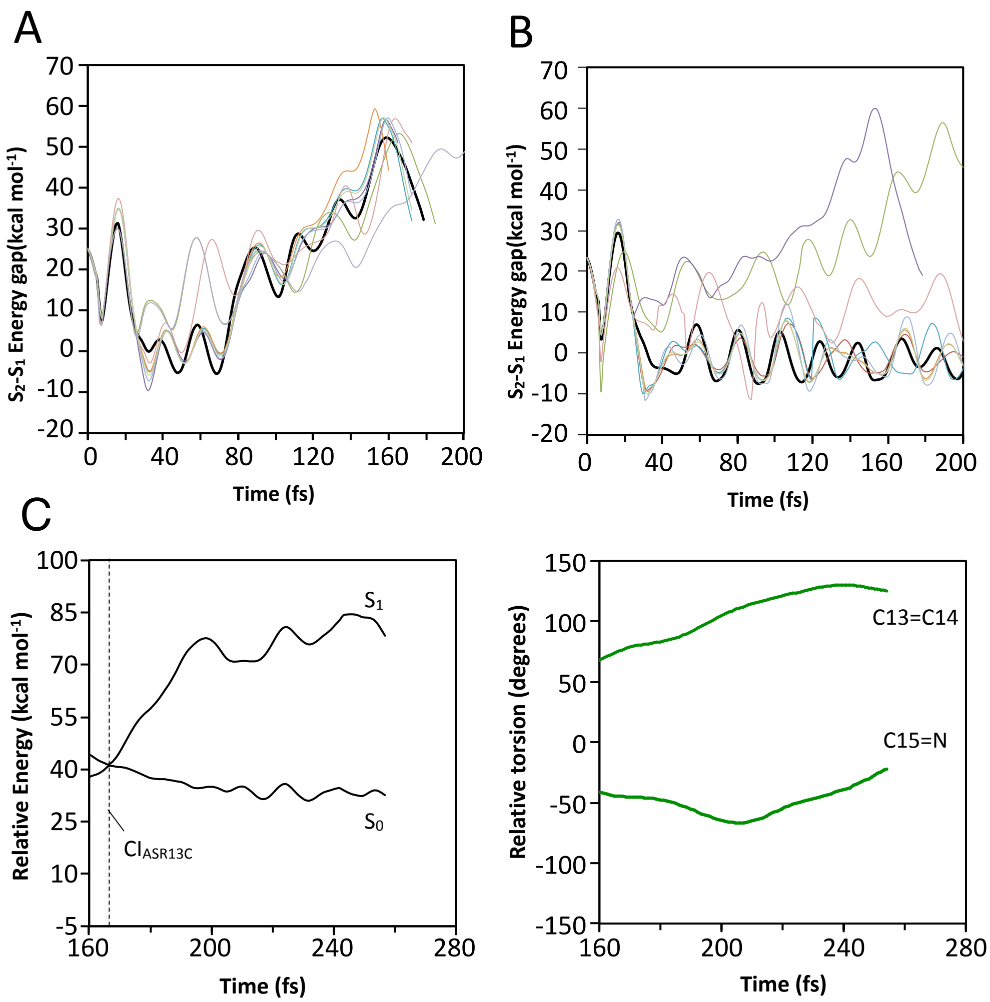

Fig. S7. S_2-S_1 CASPT2/6-31G* energy gap ($\Delta E_{S2\text{-}S1}$) computed based on multiple CASSCF/3-21G/AMBER trajectories for (A) ASR_{13C} and (B) ASR_{AT}. The thicker dark line shows the reference model which is described in the main text. (C) Energy profiles and geometrical evolution of ASR_{13C} upon ground state relaxation starting from the S_1/S_0 crossing CI_{ASR13C} reached in the trajectory of Fig. 2B (see main text). The curves display the S_0 energy relaxation (left panel) and the corresponding twisting deformations about the -NH=C15-, =C15-C14= and -C14=C13- bonds (right panel, compare with Fig. 2F) demonstrating the aborted bicycle isomerization mechanism (i.e. notice the inversion of the C15=N twisting at about 200 fs delay).

The excitation energies corresponding to the 8 optimized QM/MM models are reported, together with the original models, in Table S5. The overall average excitation energies of ASR_{13C} (53.6 kcal mol^{-1}) and ASR_{AT} (53.1 kcal mol^{-1}) reflect the same order of magnitude of the reference model. Excited state lifetimes are obtained by running CASSCF/3-21G/AMBER trajectories based on these 8 models for each isomer of ASR (the CASSCF/3-21G/AMBER level of the theory is faster yet display, for the system under investigation and for Model I energy profiles and geometrical evolution close to those of CASSCF/6-31G*/AMBER level in our ASR models according to our test calculations (see Section 1.3 above and Fig. S2). Single point CASPT2/6-31G* corrections are applied to the geometries along these trajectories to check whether a S_2/S_1 degeneracy is reached along the trajectories. This was indeed the case supporting the observations relative to the reference FC trajectories reported in the main text (only 2 trajectories in

ASR_{13C} and 1 trajectory in ASR_{AT} do not display the behavior of the corresponding reference trajectory, see Fig. S7 where we report the S_2-S_1 energy gap along the sampled trajectories). Moreover, it is shown that the average S_1 decay time is 150 fs for ASR_{13C} and >200 fs for ASR_{AT} respectively. Again, these results appear to be consistent with the FC trajectories of our reference model.

4. XMCQDPT2 Method

XMCQDPT2 energies were computed using Firefly version 8.0.0. (35) In these calculations, the intruder state avoidance (ISA) shift was set to 0.02 to avoid intruder states. Instead of the classical version of XMCQDPT2, XMCQDPT2/F(Γ_{ns}) is used. It applies a modified Fock-like operator that incorporates some terms arising due to the nonseparable part (Γ_{ns}) of the CASSCF state-averaged second-order density matrix Γ. This F(Γ_{ns}) variants has been shown to perform better than the classical version in general for PSB3 models. (36) All the calculations are based on the geometries along QM/MM trajectories with full aproprotein residues treated as point charges.

5. Analysis of the Charge Distributions along ASR_{13C} trajectory

At the FC point (S_0-min in Fig. S8) 66% of the positive charge of the S_1 state resides on the β-ionone containing moiety (we divide the chromophore in two moieties defined by cutting the full chromophore backbone at the isomerizing double bond. This is indicated with an arrow in Fig. S8). Along the FC trajectory the charge is partially transferred across the isomerizing C13=C14 bond towards the Schiff base and then it gets back as the S_1 decay region is approached. (37, 38) In Fig. S8, we detail the evolution of the charge distribution along the retinal chromophore backbone. We see that the charge originally localized on the β-ionone fragment oscillates around an average value of 60% until the S_2/S_1 near degeneracy region is entered. At around 30 fs the charge on the β-ionone fragment decreases to ca. 30-40% due to the mixing with the S_2 diradical state. However, the charge on the same β-ionone fragment then increases again when the near degeneracy region is left and and peaks to 90% when entering the S_1/S_0 conical intersection region (this is known as sudden polarization. (39)). Of course, the reference FC trajectory of ASR_{AT} shows the same features of ASR_{13C} up to the near degeneracy region that is never left.

6. Transition State Optimization

The transition states were optimized using the restricted-step rational-function-optimization method at the CASSCF/6-31G*/AMBER level of theory. (40) Since QM/MM frequency analysis is unavailable in MOLCAS/Tinker, initial attempts to optimize a transition state had to rely on a guess Hessian computed at a suitable guess structure. The quality of the Hessian is evaluated by looking at the reaction vector, thus making sure that it describes the expected isomerization motion connecting the cis to trans or trans to cis structures. The optimizations were considered completed after convergence to a stationary point and the corresponding final updated transition vector represents the expected space-saving bicycle-pedal motion. All energy barriers are reported relative to the ASR_{13C} or ASR_{AT} ground state optimized structure and are computed at the CASPT2//CASSCF/6-31G*/AMBER level of theory. In this case, CASPT2 with the default IPEA value of 0.25 (24) was used since it has been shown to be more accurate for evaluating energy barriers, (25) (but not vertical excitation energies, as discussed above, since the factors leading to a cancellation of errors in the case of vertical excitation energies no longer apply at the transition states). For more details, we refer the reader to ref. (25) where the use of the CASPT2//CASSCF protocol was benchmarked for a reduced model of the retinal protonated Schiff base).

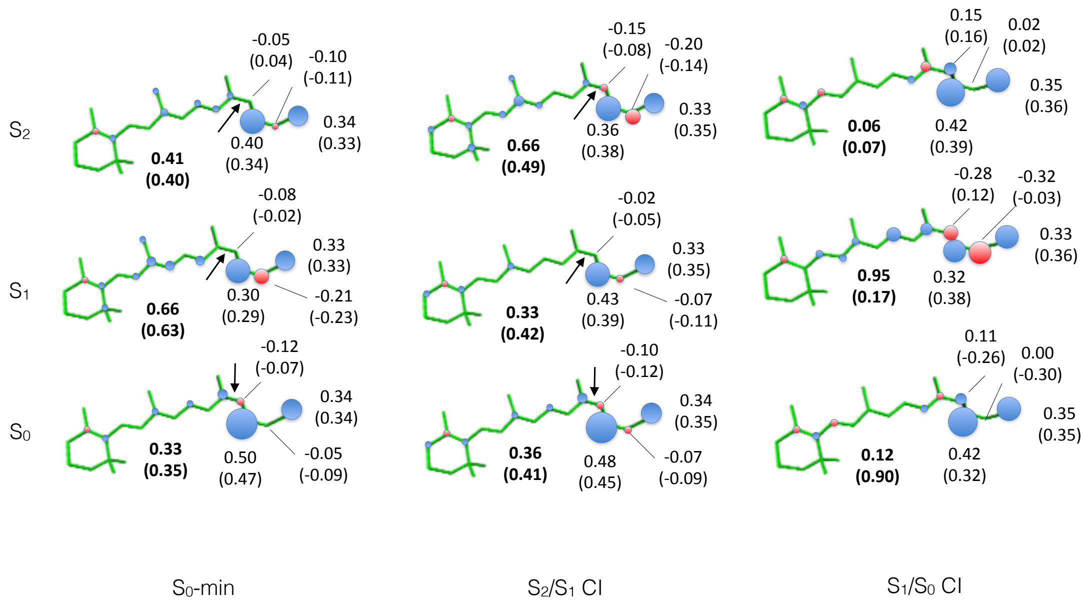

Fig. S8. Charge distribution along the ASR_{13C} chromophore backbone for the lowest three electronic states (with charges summed on heavy atoms. Circles are only shown for absolute values of the CASSCF charges larger than 0.05). These charge distributions are shown for the ground state equilibrium structure (S_0-min), a snapshot selected from the trajectories which gives an S_2/S_1 degeneracy (S_2/S_1 CI) at 30 fs and S_1/S_0 CI stucture at hop time. The charge residing on the β-ionone ring fragment is reported in bold. XMCQPT2 charges are reported in parenthesis. The arrow indicates the isomerizing C13=C14 bond.

Fig. S9 reports the geometries of the transition states for ASR_{13C} and ASR_{AT}. By comparing the TS_{CT} and TS_{DIR} structures for $ASR_{13C,}$ it is found that both transition states show a ~90° twisted C12-C13-C14-C15 dihedral angle and have similar torsional deformations. However, they mediate different electronic processes. TS_{CT} is responsible for a heterolytic C13=C14 breaking accompanied by a translocation of the positive charge with respect to the equilibrium structure, while TS_{DIR} is responsible for a homolytic C13=C14 breaking without any charge transfer. TS_{CT} has an inverted BLA pattern with respect to the reactant (BLA of TS_{CT} = 0.003 versus a BLA of reactant = 0.110), while TS_{DIR} would have a BLA pattern more similar to that of the reactant (BLA of TS_{DIR} = 0.028). We find that TS_{CT} has a computed activation energy of 30 kcal mol^{-1} and lies 20 kcal mol^{-1} below $TS_{DIR.}$ Hence, the thermal isomerization would be fully controlled by the TS_{CT}, just like in Rh. (1) Both transition states would lead to the same product, ASR_{13C}-K, which has an all-*trans*, 15-*syn* configuration. This ASR_{13C}-K has a computed excitation wavelength of 568 nm, which is red-shifted with respect to $ASR_{13C.}$ The oscillator strength value is found to be higher than that of ASR_{13C} (1.36 in ASR_{13C}-K when compared to 0.94 in ASR_{13C}). These results are both consistent with the changes in absorbance reported by Kandori and coworkers. (30)

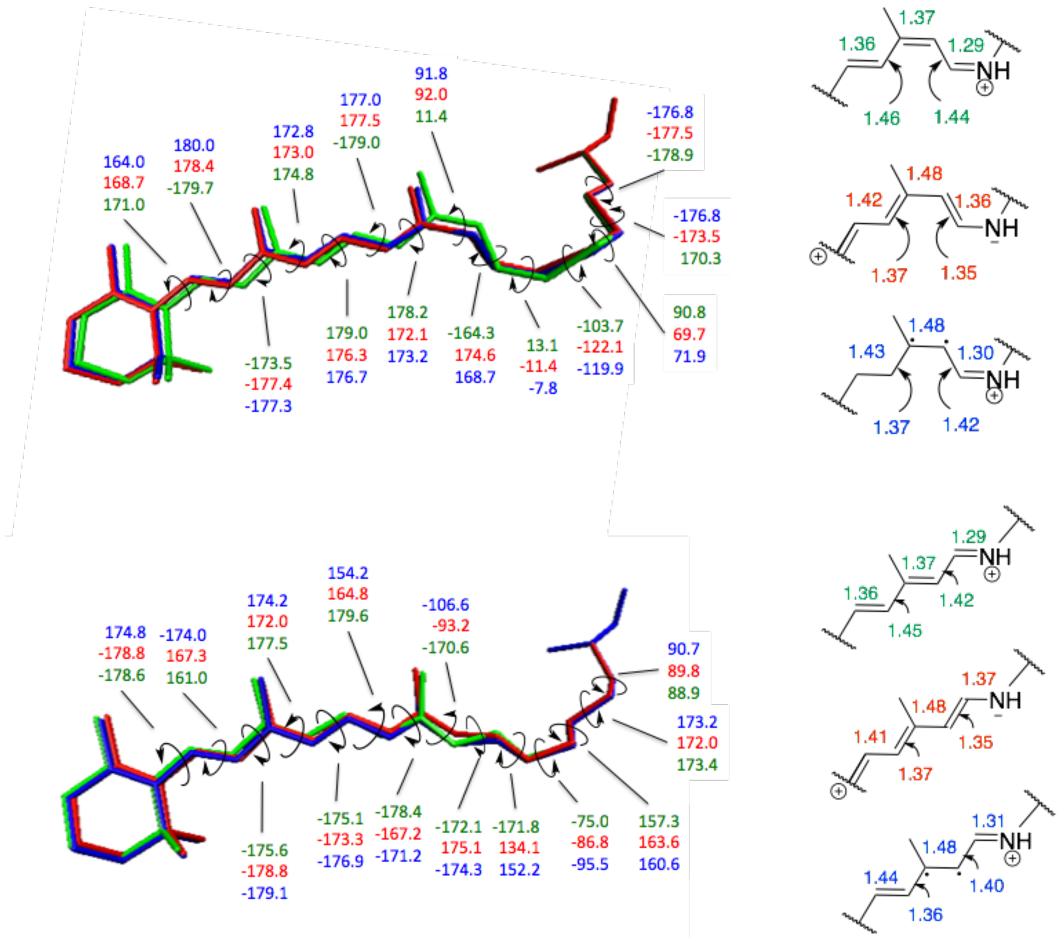

Fig. S9. Geometries of the reactant (green), charged transfer transition state (TS_{CT}, red) and diradical transition state (TS_{DIR}, blue) for ASR_{13C} (top) and ASR_{AT} (bottom). The relevant bond lengths and backbone dihedral angles are given in Å and degrees, respectively. The TS_{DIR} geometry shown for ASR_{AT} is actually the geometry of the S_1 minimum.

For ASR_{AT}, TS_{CT} leads to the ASR_{AT}-K intermediate, and has an activation energy of 28 kcal mol^{-1} and shows a 93° C12-C13-C14-C15 dihedral angle. This ASR_{AT}-K has a computed excitation wavelength of 556 nm, which is red-shifted with respect to ASR_{AT}. The oscillator strength is found to be lower than that of ASR_{AT} (1.06 in ASR_{AT} compared to 0.85 in ASR_{AT}-K). These results are also both consistent with the changes in absorbance reported by Kandori and co-workers. (30) Attempts to locate a TS_{DIR} have not been successful. This is likely due to the S_1/S_0 conical intersection topology, which is usually peaked and lies between TS_{CT} and TS_{DIR}, but in this case may be sloped instead. (25) This hypothesis is confirmed by the fact that we optimized a twisted excited state minimum in the vicinity of the conical intersection region (see Fig. S9). When considering this minimum as corresponding to TS_{DIR}, its computed activation energy barrier is 53 kcal mol^{-1}. Fig. S10 shows the charge distribution of the located transition states. This further confirms the different electronic character between the TS_{CT} and TS_{DIR}.

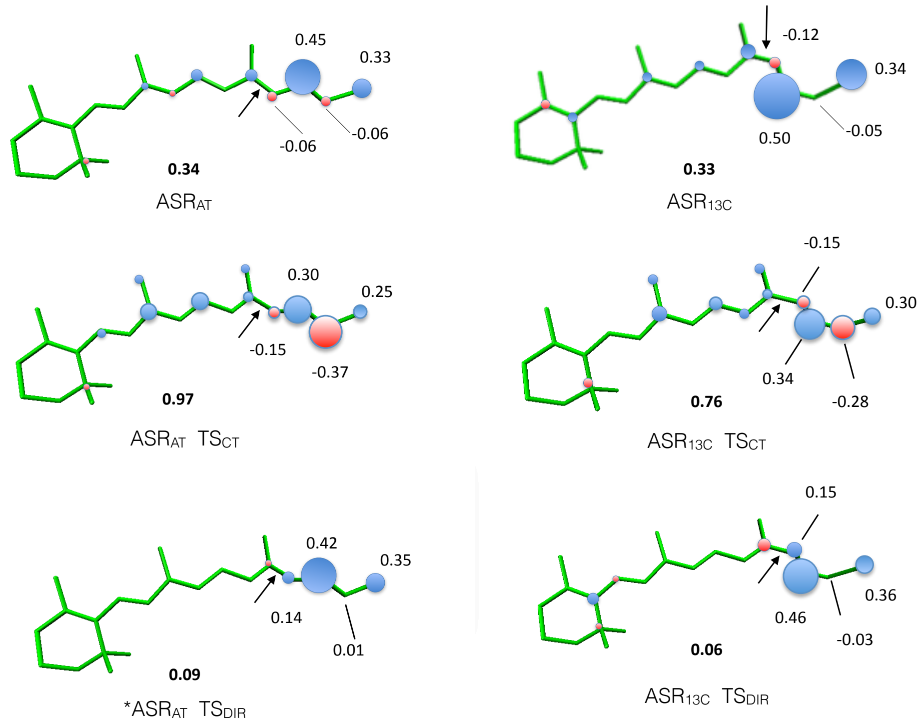

Fig. S10. Charge distribution of ASR_{13C} and ASR_{AT} chromophores for the ground state equilibrium structure, the charge transfer transition states (TS_{CT}) and diradical transition state (TS_{DIR}). Charges have been summed on heavy atoms, and circles are only shown for absolute value of CASSCF charges larger than 0.05. The charge residing on the β-ionone ring fragment is reported in bold. The arrow indicates the isomerizing C13=C14 bond. The TS_{DIR} geometry shown for ASR_{AT} is actually the geometry of the S_1 minimum.

7. Thermal Isomerization barriers.

Recently we have reported on the geometrical and electronic structure of the transition states controlling the S_0 thermal isomerization of Rh. (1, 41). Two transition states have been located featuring a charge transfer (TS_{CT}) and a covalent (TS_{DIR}) PSB11 electronic structure respectively. Although analogue PSB11 transition states have been located in squid rhodopsin (sqRh) and human melanopsin (hMeOp) as well as in Rh mutants, (1, 41) they have never been computed for PSBAT or PSB13C hosting rhodopsins. Here, we report the TS_{CT} and TS_{DIR} structures (see Fig. S9) for both ASR forms. These feature the same ~90° twisted reactive bond (i.e. C13=C14) and a BLA pattern consistent with an heterolytic double bond breaking (see Fig. S11) accompanied by a translocation of the positive charge (with respect to the S_0 equilibrium structure) for TS_{CT} and a homolytic breaking without charge transfer for TS_{DIR}. As found for Rh, sqRh and hMeOp, TS_{CT} is, with respect to TS_{DIR}, always lower in energy with computed E_a^T barriers of 28 and 30 kcal mol^{-1} for ASR_{AT} and for ASR_{13C} respectively. Starting from the TS_{CT} of ASR_{AT} it is possible to compute, via S_0 geometry optimization, a ASR_{AT}-K model featuring an all-*trans*, 15-*anti* PSB13 configuration and with a predicted 556 nm λ^a_{max} (i.e. red-shifted relative to ASR_{AT}). This is consistent with the changes in absorbance reported by Kandori and co-workers during the photochemical formation of AS-R_{AT}-K. (30) The same is true for ASR_{13C}.

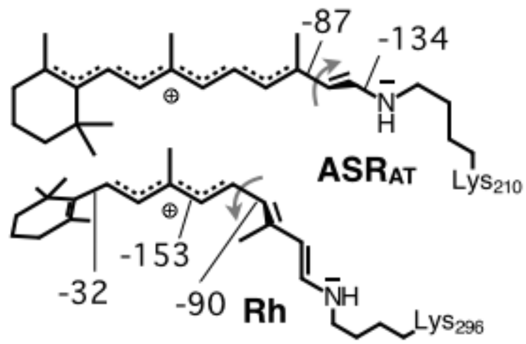

Fig. S11. Schematic representation of the TS_{CT} structures of ASR_{AT} and Rh together with their main out-of-plane (deviation larger than ±5°) dihedrals given in degrees.

The findings above are consistent with those reported for Rh where a TS_{CT} featuring a ~90° twisted C11=C12 bond controls the thermal formation of bathoRh. (1) However, the computed E_a^T values of ASR_{13C} and ASR_{AT} are ca. 5 and 7 kcal mol^{-1} lower with respect to the Rh value, respectively. This difference can, again, be explained on the basis of the distinctive features of the Rh chromophore. In fact, as schematically shown in Fig. 4, the TS_{CT} structure of Rh offers limited space (i.e. the C6-C7=C8-C9=C10 fragment) for the delocalization of the translocated positive charge with respect to the ASR_{AT} chromophore. Such confinement is a consequence of the β-ionone ring partial twisting on one side and fully twisted C11=C12 bond on the other side of the PSB11 backbone.

8. Effect of the State-Averaging with Three and Four Roots.

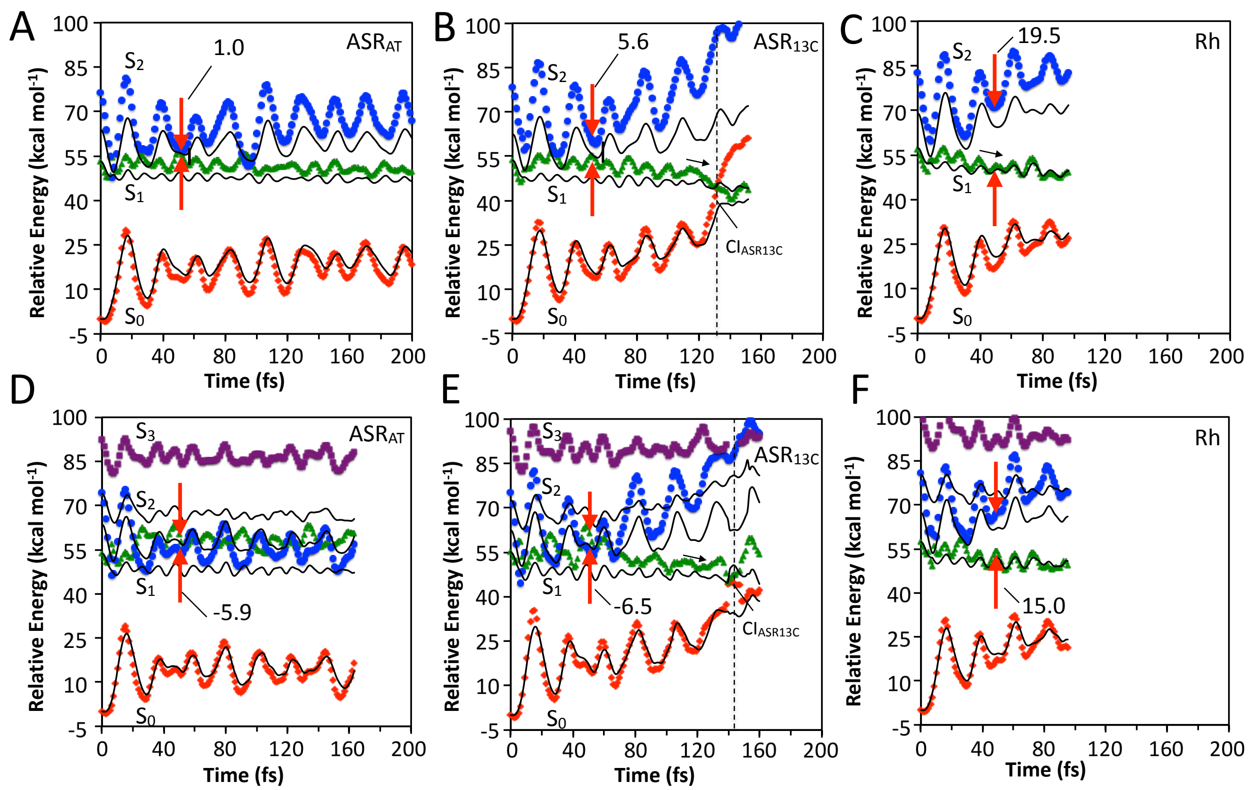

Fig. S12. Three and four state-averaged QM/MM trajectories of ASR_{AT}, ASR_{13C} and Rh computed at the scaled-CASSCF/Amber (black lines) level of theory and corrected at the CASPT2 level. The numbers reported on the "double arrow" symbol are the values of the S_2-S_1 energy gap (kcal mol^{-1}) at 60 fs dynamics. (A) Three root state average S_0 (full diamonds), S_1 (full triangles) and S_2 (full circles) CASPT2//CASSCF/Amber energy profiles along the ASR_{AT} trajectory. (B) Same data for the ASR_{13C} trajectory and (C) for the Rh trajectory. (D) Four root state average S_0 (full diamonds), S_1 (full triangles), S_2 (full circles) and S_3 (full squares) CASPT2//CASSCF/Amber energy profiles along the ASR_{AT} trajectory. (E) Same data for the ASR_{13C} trajectory and (F) for the Rh trajectory.

9. Cartesian Coordinates of the QM subsystem of stationary points reported in this work.

ASR_{13C}
C 32.35706262 23.10470274 21.69796305
C 33.69531106 23.56803257 21.07612992
C 34.28125497 24.87667686 21.66568974
H 31.64021385 23.92689394 21.70050059
H 32.53046767 22.79894352 22.73018665
H 34.43636631 22.77925262 21.18793438
H 33.52377934 23.68263312 20.00882996
H 33.45560985 25.55297215 21.89751141
H 34.78157790 24.64123142 22.60783619
C 35.25343506 25.60607734 20.75215820
N 34.57512092 25.85017425 19.47622959
H 35.54297236 26.54292425 21.20952807

H 36.12337488 24.99190633 20.58155509
H 33.59376298 26.02165506 19.57001137
C 41.07333967 29.63867030 9.89407083
C 41.63518972 30.52074730 8.75664342
C 42.83667415 29.90131617 8.05863715
C 42.40627898 28.60494361 7.39188557
C 41.51395138 27.74282999 8.26252306
C 40.93439870 28.17491166 9.41744602
C 40.15160689 27.18937319 10.20751761
C 39.82146511 27.22211077 11.52203510
C 39.05946320 26.19940336 12.24507181
C 38.77464885 26.44576788 13.55861918
C 37.92584065 25.65360090 14.40928042
C 37.64578879 25.96997618 15.70721965
C 36.59102094 25.34599428 16.46134456
C 36.32292718 25.75249596 17.75305365
C 34.99191565 25.72702106 18.25877937
C 42.02221002 29.74421798 11.10533370
C 39.70189339 30.24150108 10.26307709
C 41.31828870 26.33873892 7.70940236
C 38.62104304 24.95887004 11.50086811
C 35.78203473 24.24170049 15.81903109
H 41.87826032 31.49913513 9.15870169
H 40.85383442 30.68042673 8.01581841
H 43.63292267 29.70544730 8.77062715
H 43.24090784 30.58177245 7.31617298
H 43.27950613 28.02236653 7.10649195
H 41.88774363 28.82231047 6.45868079
H 39.84878874 26.31733576 9.66092528
H 40.10693397 28.05742278 12.12654169
H 39.16238828 27.35034267 13.99616452
H 37.44623069 24.80150438 13.97192629
H 38.14303074 26.80612982 16.16606851
H 37.04804391 26.32139329 18.30353192
H 34.19792221 25.73011556 17.53715337
H 41.64533154 29.23737837 11.98289226
H 42.99620571 29.31980800 10.88971136
H 42.16070402 30.78987185 11.36828117
H 39.27607739 29.82093987 11.16436307
H 39.80312058 31.31118010 10.41560032
H 38.98510022 30.09434241 9.46063989
H 41.82570437 26.24213614 6.75679408
H 41.71783577 25.57223090 8.36528579
H 40.27278268 26.10216432 7.53452416
H 37.93469745 25.20373930 10.69710773
H 39.48187023 24.46867963 11.05908135
H 38.13719831 24.23472784 12.13863418
H 36.40742414 23.36074419 15.71879505
H 34.92894554 23.95276866 16.41953246
H 35.42866500 24.51061688 14.83379673
H 34.53985488 25.07069739 21.42269035

ASR_{13C} TS_{CT}

C 32.31148573 23.11516416 21.70270037
C 33.59598377 23.67317065 21.06297460
C 34.20731147 24.83834288 21.85443682
H 31.55495512 23.90024866 21.74686406
H 32.53056722 22.79234975 22.72068483
H 34.33754341 22.87810216 20.99973484
H 33.36498877 24.00809902 20.05189553
H 33.44211811 25.59286233 22.03986059
H 34.55960275 24.46678235 22.81763882
C 35.37578296 25.46321436 21.11223863
N 34.92079020 26.16930995 19.94633729
H 35.90014788 26.12417223 21.79154379
H 36.05743483 24.67231499 20.83654689
H 34.49742302 27.05530646 20.11312859
C 40.81411858 29.69503832 10.28878531
C 41.32949015 30.58166380 9.13208219
C 42.52506147 29.98423571 8.40753534
C 42.10056657 28.67942152 7.75370092
C 41.24939997 27.79629988 8.64142004
C 40.71100142 28.22085677 9.82947190
C 40.04176445 27.20426691 10.64478456
C 39.59794612 27.25903785 11.93893832
C 38.92061647 26.19444148 12.62368003
C 38.49294397 26.45710584 13.92986439
C 37.70491489 25.58640061 14.67003105
C 37.33113269 25.81026143 16.01649619
C 36.51051158 24.97263369 16.73255961
C 36.31429377 25.19162401 18.18491523
C 35.29893513 25.95014232 18.65635576
C 41.77645334 29.83555351 11.48611831
C 39.42344908 30.25430026 10.65859987
C 41.06829464 26.40032594 8.06277907
C 38.67987264 24.84028052 11.99747042
C 35.82465188 23.76675222 16.12632183
H 41.56309129 31.56552721 9.52428989
H 40.52569370 30.72160760 8.41170691
H 43.34429823 29.80682386 9.09751181
H 42.89502196 30.66934929 7.65274671
H 42.97068541 28.11110794 7.43369136
H 41.54143203 28.88524099 6.84162989
H 39.91143297 26.26772434 10.14728964
H 39.72132789 28.15173511 12.51459208
H 38.76263099 27.39873142 14.37504524
H 37.37242490 24.68120562 14.20353916
H 37.73676752 26.67373798 16.51025378
H 37.04571726 24.75977564 18.84702368
H 34.67017332 26.46496137 17.94978885
H 41.44190264 29.29371150 12.36215456
H 42.76819156 29.47018109 11.24512154
H 41.86489392 30.88111763 11.76403281
H 39.02343954 29.85573005 11.58143484

H 39.48836853 31.33032037 10.77676369
H 38.70287793 30.05761600 9.87032999
H 41.36529956 26.40153730 7.02094850
H 41.68572619 25.66370361 8.56698444
H 40.04195900 26.05286691 8.09721858
H 38.97173807 24.79971842 10.96130763
H 39.24712100 24.08835124 12.53674626
H 37.63001168 24.57877411 12.04285158
H 36.46438371 22.89068300 16.20978264
H 34.92118382 23.55505319 16.68162968
H 35.55361719 23.89714785 15.08677907
H 34.51812489 25.00455870 21.65701210

ASR_{13C}-K
C 32.29981153 23.13371086 21.68328482
C 33.57886485 23.70888688 21.03908830
C 34.14019942 24.91025972 21.80845890
H 31.53121485 23.90720042 21.72368475
H 32.52321029 22.82338201 22.70455846
H 34.33475058 22.92463155 21.02263217
H 33.37526420 24.01797751 20.01355534
H 33.45654300 25.75395085 21.71892682
H 34.20559812 24.63732245 22.86510959
C 35.53064506 25.27447149 21.33425199
N 35.52939479 26.32600037 20.31495526
H 36.09260737 25.67824350 22.16083395
H 36.02835988 24.39737097 20.95738341
H 35.58080094 27.26719700 20.68416939
C 40.64075044 29.54967555 10.51064308
C 41.17300161 30.39113703 9.32774158
C 42.31930431 29.72606586 8.58333356
C 41.80954506 28.43425448 7.96468517
C 40.95402175 27.60673282 8.90466591
C 40.47493948 28.06746397 10.10503319
C 39.81041839 27.08978211 10.98923583
C 39.36550236 27.18866388 12.28205536
C 38.72537080 26.12007276 13.04568780
C 38.18978549 26.42463696 14.27886872
C 37.43897005 25.49410994 15.07702828
C 36.90383962 25.74708337 16.31690691
C 36.13930253 24.76198993 17.06165704
C 35.65422363 24.94953255 18.32628205
C 35.69420946 26.20281101 19.04701854
C 41.62167118 29.68826888 11.69314876
C 39.27775618 30.17349307 10.87814042
C 40.69480991 26.20456869 8.37339976
C 38.65911919 24.69676725 12.51740424
C 35.87192441 23.41335845 16.42494665
H 41.46123045 31.37057952 9.69620115
H 40.36069741 30.55874150 8.62270589
H 43.14376226 29.51497487 9.25860603
H 42.70490500 30.38266170 7.80948446

H 42.64270945 27.82099073 7.62695596
H 41.23605037 28.65929923 7.06519470
H 39.69137806 26.12906640 10.53571419
H 39.44158905 28.11697442 12.81300085
H 38.28840335 27.42932365 14.65427455
H 37.28933250 24.52025228 14.65508877
H 37.08211305 26.71087010 16.75897161
H 35.16415868 24.13223515 18.81923336
H 35.81933393 27.13095995 18.52287733
H 41.29119270 29.14312657 12.56797400
H 42.60683161 29.31570753 11.43483713
H 41.72230547 30.73421810 11.97200327
H 38.86576504 29.80196506 11.80608489
H 39.38825678 31.24931514 10.97666525
H 38.54653976 29.99296388 10.09578958
H 40.96130316 26.15668242 7.32275221
H 41.28684647 25.45056572 8.88408795
H 39.65503723 25.90722236 8.44839673
H 39.05731334 24.60606689 11.51909547
H 39.23998646 24.03696179 13.15425426
H 37.63789578 24.33136174 12.48247880
H 36.79374694 22.89962587 16.18144281
H 35.29629515 22.77737412 17.08566278
H 35.31247856 23.53829608 15.50550039
H 34.51005796 25.00714005 21.68231986

ASR_{13C} TS_{DIR}
C 32.31203243 23.11987338 21.70113284
C 33.59448765 23.70560663 21.07253389
C 34.19249212 24.86374702 21.89111458
H 31.54717056 23.89631101 21.75424945
H 32.53243647 22.79257191 22.71753947
H 34.34300774 22.91776110 20.99904212
H 33.36665926 24.05774048 20.06634412
H 33.42467084 25.62106780 22.05854227
H 34.49149169 24.47622433 22.86827070
C 35.40622054 25.48575825 21.22878433
N 35.00141453 26.25940218 20.05831827
H 35.88966176 26.16797407 21.91416436
H 36.09312897 24.71061939 20.94320049
H 34.41254180 27.05481899 20.24995050
C 40.74284342 29.61642482 10.30019706
C 41.25548599 30.52176139 9.15742516
C 42.45058995 29.93836228 8.42104256
C 42.03231279 28.63649063 7.75584307
C 41.17841446 27.74618728 8.63790830
C 40.61857148 28.15216448 9.81765338
C 39.88770091 27.14266428 10.61128462
C 39.48670241 27.16302236 11.92315949
C 38.77173416 26.10414374 12.58903159
C 38.38450623 26.31019837 13.92627728
C 37.57348712 25.48024207 14.69844618

C 37.28518974 25.73461416 16.07737820
C 36.44776532 24.97579524 16.85365830
C 36.32872739 25.22924993 18.30233355
C 35.34245796 26.10826129 18.81562193
C 41.71945478 29.72415473 11.49099510
C 39.36666296 30.18938321 10.69971749
C 41.00343005 26.34710654 8.06435704
C 38.42400806 24.83784644 11.83866360
C 35.69230381 23.77052352 16.31539566
H 41.48844570 31.50161264 9.56204306
H 40.44963008 30.66961996 8.44020672
H 43.27148004 29.75867364 9.10885994
H 42.81733608 30.63709975 7.67566986
H 42.90956228 28.07621421 7.43981445
H 41.48402241 28.85198449 6.83848883
H 39.66713180 26.24059839 10.07734583
H 39.69021183 28.01957835 12.53438081
H 38.73364167 27.21724253 14.39343991
H 37.14703528 24.60394821 14.25321423
H 37.77621517 26.57940042 16.53102125
H 37.02938898 24.78387719 18.98789253
H 34.84337929 26.77129868 18.13418480
H 41.83822314 30.76530238 11.77952678
H 41.37433258 29.17906077 12.36016436
H 42.69915233 29.33389849 11.23941150
H 38.96439903 29.75692203 11.60541447
H 39.45340125 31.26021866 10.85740129
H 38.63897461 30.03584360 9.90828817
H 41.52449633 25.59364861 8.64680754
H 39.96311153 26.04509453 8.00119992
H 41.40576864 26.30699007 7.05786917
H 39.29747301 24.44852082 11.32692581
H 38.07531932 24.05593993 12.49773618
H 37.65421822 25.01375287 11.09224738
H 35.21203587 23.99638390 15.37165855
H 36.35935636 22.92789517 16.15985206
H 34.91851063 23.44889892 17.00533489
H 34.51534388 25.02920201 21.71493473

ASR_{AT}
C 32.15731488 23.25965839 21.79268384
C 33.57215669 23.85388163 21.66859791
C 33.73737548 24.96441662 20.63028610
H 31.40761608 24.04448982 21.70144445
H 32.10076727 22.90987438 22.82605164
H 33.83676790 24.27317996 22.64160877
H 34.27771531 23.05536199 21.44171892
H 33.59378070 24.52921040 19.63798089
H 32.98814716 25.73796557 20.79827379
C 35.11317049 25.57804271 20.77161922
N 35.55019575 26.19740548 19.51023009
H 35.09811318 26.33238065 21.54093671

H 35.82723260 24.81376658 21.03517956
H 35.60470750 27.21085936 19.48519240
C 41.18207050 29.71402505 9.74829967
C 41.81064085 30.69058943 8.72938562
C 43.03951679 30.12629191 8.03539060
C 42.61965800 28.91615208 7.21921471
C 41.71629255 27.96660748 7.98047396
C 41.08066223 28.28967629 9.14959152
C 40.32624766 27.23182362 9.84348475
C 39.81411083 27.23898506 11.11094052
C 39.11082320 26.15493949 11.77271814
C 38.69113191 26.40678111 13.05967241
C 37.92778894 25.57573098 13.93634703
C 37.56178034 26.04272303 15.17858715
C 36.78474495 25.35450077 16.16441621
C 36.50022679 26.05829371 17.31300769
C 35.92307155 25.50758034 18.49334604
C 42.05587653 29.71146778 11.01982548
C 39.79282466 30.30346505 10.07351152
C 41.60867468 26.60791688 7.31130137
C 38.84088826 24.86318777 11.03698002
C 36.27789221 23.95786103 15.88170474
H 42.03542522 31.62606055 9.23222700
H 41.07173501 30.92759197 7.96613359
H 43.79780951 29.84511268 8.76070304
H 43.48475584 30.87384529 7.38610383
H 43.49535688 28.37058187 6.87483662
H 42.11189810 29.24529382 6.31309401
H 40.20585875 26.31956514 9.29444570
H 39.92972692 28.10773970 11.72214611
H 38.94109237 27.37268327 13.46605170
H 37.62850644 24.59571021 13.61672091
H 37.87356916 27.03825550 15.44180539
H 36.80295442 27.08461413 17.36697944
H 35.81152439 24.44447515 18.59596188
H 41.64833890 29.09915151 11.81211167
H 43.05393050 29.33911537 10.81527648
H 42.14692454 30.72528763 11.40223737
H 39.30475210 29.83809518 10.91794110
H 39.89154769 31.36126618 10.29545095
H 39.12752934 30.21323728 9.22083839
H 41.85399679 26.70976288 6.25926299
H 42.31005801 25.89202689 7.73507363
H 40.61976400 26.16927603 7.36290082
H 39.76138064 24.44363805 10.64329281
H 38.39186931 24.11251142 11.67279269
H 38.17024425 25.02727216 10.19870853
H 37.06779541 23.33203792 15.48787649
H 35.86545772 23.46513023 16.75342068
H 35.49383645 24.01196604 15.13480351
H 34.10333696 25.12764116 20.66788071

ASR_{AT} TS_{CT}

C 32.17714652 23.25627307 21.78602973
C 33.61253200 23.79925913 21.65954598
C 33.82339667 24.88636405 20.60872008
H 31.45299318 24.06246413 21.68166711
H 32.10438049 22.91841590 22.82198149
H 33.88829086 24.22360834 22.62702788
H 34.29169251 22.97580699 21.44424811
H 33.67628819 24.45441232 19.61707762
H 33.10442144 25.69046562 20.76310179
C 35.22682095 25.45564852 20.73833827
N 35.61627479 26.19061616 19.57274916
H 35.26176573 26.08769003 21.61389549
H 35.91766361 24.63408183 20.88995939
H 35.21944470 27.09640183 19.44089865
C 41.08059008 29.72415045 9.89025784
C 41.66269723 30.65873383 8.80581923
C 42.88067362 30.07742415 8.10531454
C 42.45450254 28.82380631 7.36131320
C 41.59344555 27.89265970 8.18832839
C 41.00006410 28.26975063 9.36534446
C 40.31963780 27.22697910 10.13581682
C 39.85995587 27.26220688 11.42206123
C 39.22320922 26.16473003 12.09325191
C 38.79912409 26.40539308 13.39973727
C 38.02737109 25.53322258 14.15537324
C 37.50623685 25.87781936 15.42159412
C 36.50937012 25.16725284 16.04294729
C 35.83881795 25.75929494 17.21710213
C 36.19027750 25.55729365 18.50517861
C 41.98315298 29.81040195 11.13787061
C 39.67897311 30.28262909 10.21617145
C 41.49302309 26.51348836 7.55917603
C 39.00048174 24.85241883 11.38298449
C 35.95167170 23.86108404 15.52350425
H 41.88745654 31.61748700 9.26004195
H 40.89886209 30.85040110 8.05519697
H 43.66512995 29.84326692 8.81851368
H 43.29553764 30.79382249 7.40505222
H 43.32051853 28.27171577 7.00528016
H 41.90132097 29.09870462 6.46439934
H 40.20344755 26.29345712 9.62627641
H 39.95564256 28.15006768 12.00717564
H 39.02469106 27.36457666 13.83116552
H 37.75783769 24.58501662 13.73887795
H 37.80901373 26.81437967 15.85431392
H 34.95295299 26.33383065 17.00079402
H 36.98309209 24.86806967 18.75656253
H 41.60738044 29.24739752 11.98155281
H 42.98214338 29.44224590 10.93329087
H 42.06558919 30.84680791 11.45071747
H 39.21927020 29.83935891 11.08956806

H 39.75135492 31.34891189 10.39893631
H 39.00178225 30.14279186 9.37935240
H 41.62310992 26.60787396 6.48674786
H 42.28415225 25.85829275 7.91470880
H 40.54707207 26.01267405 7.71963801
H 39.91054804 24.54284240 10.88662818
H 38.72051994 24.05697842 12.05414832
H 38.22405866 24.95984622 10.63218422
H 36.66921863 23.27264676 14.96736218
H 35.60555530 23.26113238 16.35430298
H 35.09721967 24.05136854 14.87915830
H 34.19670753 25.03779372 20.64319852

ASR_{AT}-K
C 32.15860975 23.25716637 21.79242422
C 33.59263507 23.80007160 21.69753009
C 33.83882577 24.87549847 20.64448506
H 31.43649031 24.06292449 21.67368616
H 32.06774228 22.92220445 22.82834089
H 33.84018257 24.23226233 22.66929531
H 34.27641364 22.97466252 21.50777152
H 33.75758447 24.42873393 19.65177743
H 33.10553488 25.67499892 20.74874495
C 35.22757774 25.44846385 20.86907749
N 35.69643737 26.20583005 19.74084950
H 35.20350139 26.07098634 21.75056675
H 35.91270605 24.62943175 21.05761764
H 35.20648927 27.05805749 19.55582848
C 40.91398915 29.79877069 10.08484482
C 41.44937506 30.74017298 8.98214869
C 42.68320683 30.19416008 8.28046956
C 42.29782533 28.91995368 7.54785728
C 41.47049142 27.96959080 8.38893790
C 40.89267550 28.33479596 9.57706181
C 40.28831182 27.26898361 10.36537835
C 39.80629424 27.29303302 11.64812708
C 39.23490125 26.17320550 12.31383726
C 38.69651165 26.41922741 13.58624374
C 37.92427912 25.51602216 14.29209217
C 37.31553230 25.85748057 15.52551347
C 36.39615282 25.09166256 16.18910862
C 35.74412902 25.68670338 17.38348460
C 36.16233478 25.50659210 18.64475672
C 41.81514681 29.94597630 11.32858825
C 39.48799456 30.29565438 10.40747049
C 41.38931992 26.58805455 7.75697568
C 39.16216030 24.80736238 11.67550143
C 35.89688706 23.74205956 15.75160254
H 41.63896485 31.71438363 9.41825925
H 40.67271965 30.89084283 8.23526158
H 43.47603747 29.99029268 8.99324551
H 43.07483050 30.91896781 7.57598737

H 43.18152134 28.39027481 7.20119201
H 41.73678510 29.16513162 6.64778976
H 40.24891722 26.31856492 9.87798895
H 39.81729701 28.19816486 12.21443147
H 38.82770099 27.40136499 14.00677842
H 37.74260829 24.54473549 13.87851856
H 37.55303634 26.82072862 15.94254744
H 34.93932662 26.37550672 17.17315727
H 36.94219245 24.79688952 18.87716440
H 41.44744093 29.40323600 12.18984392
H 42.82166217 29.59211132 11.13508850
H 41.87520638 30.99271521 11.61093253
H 39.05821291 29.85270384 11.29656646
H 39.51106749 31.36868648 10.56359473
H 38.81153420 30.10236726 9.58040584
H 41.47843506 26.69201868 6.68152324
H 42.20922061 25.95348531 8.08119793
H 40.46185274 26.06341259 7.94591007
H 40.01660625 24.63474142 11.03671894
H 39.16184624 24.02321746 12.41574716
H 38.26127556 24.72800848 11.07369266
H 36.41555708 23.31172603 14.90727287
H 35.96372581 23.04560932 16.58121677
H 34.84382373 23.82362747 15.49456321
H 34.20823379 25.02790726 20.70422664

ASR_{AT} TS_{DIR} (S_1 min)
C 32.17103572 23.25531321 21.79726074
C 33.60491508 23.81958918 21.70923224
C 33.80102094 24.96081997 20.71329362
H 31.43966400 24.05526845 21.69282826
H 32.08502156 22.90930916 22.82975141
H 33.87090383 24.20233287 22.69646846
H 34.29485147 23.01535835 21.45773617
H 33.63426787 24.55528582 19.71084108
H 33.05741325 25.73584748 20.90103856
C 35.18674496 25.56896633 20.82055614
N 35.49373858 26.24107251 19.56509120
H 35.21665597 26.27725849 21.63296720
H 35.91473855 24.78914089 20.97850710
H 35.00477295 27.10786307 19.38058479
C 41.12711665 29.73162098 9.81911166
C 41.72149044 30.68410962 8.75631021
C 42.94140860 30.11049636 8.05356126
C 42.50625108 28.88188171 7.27431561
C 41.66090751 27.93350822 8.09900904
C 41.08537062 28.27537530 9.29595901
C 40.47232764 27.20474974 10.08871057
C 39.95582619 27.24666790 11.36738951
C 39.45361691 26.15441796 12.12574793
C 38.90214527 26.45830810 13.39867504
C 38.23402829 25.57430171 14.21526160

C 37.63743985 25.99256559 15.45729563
C 36.63336281 25.35163654 16.11564072
C 35.98268011 26.02378155 17.25533829
C 36.18212049 25.68964468 18.59981973
C 41.99004161 29.83517054 11.09325205
C 39.70752827 30.26633536 10.10374717
C 41.55618407 26.55474618 7.46977887
C 39.46592570 24.72319687 11.63882780
C 35.96615816 24.06782514 15.66469143
H 41.94230552 31.63731203 9.22555466
H 40.96612850 30.88866362 8.00017931
H 43.71289102 29.84353444 8.77049207
H 43.37472706 30.84286739 7.37997343
H 43.37322892 28.34164346 6.90000410
H 41.95253037 29.18682769 6.38716586
H 40.49848444 26.23849795 9.62998704
H 39.90142455 28.18578226 11.87540622
H 38.98142108 27.47997542 13.73448078
H 38.09558240 24.56272372 13.89049950
H 37.94720508 26.95190291 15.83576575
H 35.15829777 26.68471544 17.04552778
H 36.81592399 24.86865553 18.88375979
H 41.59421497 29.26632943 11.92257305
H 42.99829776 29.47518736 10.91739898
H 42.05273905 30.87389667 11.40647119
H 39.21975793 29.79602213 10.94573513
H 39.75354720 31.33067530 10.30999765
H 39.06866614 30.12947613 9.23743173
H 40.59110347 26.08364302 7.61005892
H 41.71682072 26.64021672 6.39960517
H 42.31553799 25.87525279 7.85106101
H 39.80131608 24.05685709 12.42611722
H 38.47576450 24.40489373 11.31988641
H 40.13505911 24.59392181 10.79898776
H 36.43421423 23.64342162 14.79000330
H 35.99354945 23.31635041 16.44993055
H 34.92242162 24.24659185 15.42161123
H 34.16962353 25.12258690 20.74182545

References

1. Rinaldi S, Melaccio F, Gozem S, Fanelli F, and Olivucci M (2014) Comparison of the isomerization mechanisms of human melanopsin and invertebrate and vertebrate rhodopsins. *Proc Natl Acad Sci U S A* 111:1714-9.

2. Vogeley L, Sineshchekov OA, Trivedi VD, Sasaki J, Spudich JL, and Luecke H (2004) Anabaena sensory rhodopsin: a photochromic color sensor at 2.0 A. *Science* 306:1390-3.

3. Li H, Robertson AD, and Jensen JH (2005) Very fast empirical prediction and rationalization of protein pKa values. *Proteins: Structure, Function, and Bioinformatics* 61:704-721.

4. Olsson MH, Søndergaard CR, Rostkowski M, and Jensen JH (2011) PROPKA3: consistent treatment of internal and surface residues in empirical pKa predictions. *J Chem Theo Comput* 7:525-537.

5. Fahmy K, Jäger F, Beck M, Zvyaga TA, Sakmar TP, and Siebert F (1993) Protonation states of membrane-embedded carboxylic acid groups in rhodopsin and metarhodopsin II: a Fourier-transform infrared spectroscopy study of site-directed mutants. *Proc Natl Acad Sci U S A* 90:10206-10.

6. Yan EC, Kazmi MA, Ganim Z, Hou J-M, Pan D, Chang BS, Sakmar TP, and Mathies RA (2003) Retinal counterion switch in the photoactivation of the G protein-coupled receptor rhodopsin. *Proc Natl Acad Sci U S A* 100:9262-9267.

7. Sekharan S, and Buss V (2008) Glutamic acid 181 is uncharged in dark-adapted visual rhodopsin. *J Am Chem Soc* 130:17220-17221.

8. Frähmcke JS, Wanko M, Phatak P, Mroginski MA, and Elstner M (2010) The protonation state of Glu181 in rhodopsin revisited: interpretation of experimental data on the basis of QM/MM calculations. *J Phys Chem B* 114:11338-52.

9. Sandberg MN, Amora TL, Ramos LS, Chen MH, Knox BE, and Birge RR (2011) Glutamic acid 181 is negatively charged in the bathorhodopsin photointermediate of visual rhodopsin. *J Am Chem Soc* 133:2808-11.

10. Tomasello G, Olaso-González G, Altoè P, Stenta M, Serrano-Andrés L, Merchán M, Orlandi G, Bottoni A, and Garavelli M (2009) Electrostatic control of the photoisomerization efficiency and optical properties in visual pigments: on the role of counterion quenching. *J Am Chem Soc* 131:5172-86.

11. Roos BO, Bruna P, Peyerimhoff SD, Shepard R, Cooper DL, Gerratt J, and Raimondi M (1987) Ab Initio Methods in Quantum Chemistry, II. *Adv Chem Phys* 69:399-446.

12. Cornell WD, Cieplak P, Bayly CI, Gould IR, Merz KM, Ferguson DM, Spellmeyer DC, Fox T, Caldwell JW, and Kollman PA (1995) A second generation force field for the simulation of proteins, nucleic acids, and organic molecules. *J Am Chem Soc* 117:5179-5197.

13. Ferré N, and Olivucci M (2003) Probing the rhodopsin cavity with reduced retinal models at the CASPT2//CASSCF/AMBER level of theory. *J Am Chem Soc* 125:6868-9.

14. Ferre N, Cembran A, Garavelli M, and Olivucci M (2004) Complete-active-space self-consistent-field/Amber parameterization of the Lys296--retinal--Glu113 rhodopsin chromophore-counterion system. *Theo Chem Acc* 112:335-341.

15. Senn HM, and Thiel W (2009) QM/MM methods for biomolecular systems. *Angew Chem Int Ed* 48:1198-229.

16. Ferré N, and Ángyán JG (2002) Approximate electrostatic interaction operator for QM/MM calculations. *Chem Phys Lett* 356:331-339.

17. Melaccio F, Olivucci M, Lindh R, and Ferré N (2011) Unique QM/MM potential energy surface exploration using microiterations. *Inter J Quant Chem* 111:3339-3346.

18. Aquilante F, De Vico L, Ferré N, Ghigo G, Malmqvist PA, Neogrády P, Pedersen TB, Pitonák M, Reiher M, Roos BO, Serrano-Andrés L, Urban M, Veryazov V, and Lindh R (2010) MOLCAS 7: the next generation. *J Comput Chem* 31:224-47.

19. Ponder JW, and Richards FM (1987) An efficient newton-like method for molecular mechanics energy minimization of large molecules. *J Comput Chem* 8:1016-1024.

20. Singh UC, and Kollman PA (1986) A combined ab initio quantum mechanical and molecular mechanical method for carrying out simulations on complex molecular systems: Applications to the CH3Cl+ Cl- exchange reaction and gas phase protonation of polyethers. *J Comput Chem* 7:718-730.

21. Hermans J, Xia X, Zhang L, and Cavanaugh D (2014) Dowser program. Available at: http://danger.med.unc.edu/hermans/dowser/dowser.htm [Accessed 2014].

22. Hess B, Kutzner C, Van Der Spoel D, and Lindahl E (2008) GROMACS 4: Algorithms for highly efficient, load-balanced, and scalable molecular simulation. *J Chem Theo Comput* 4:435-447.

23. Andersson K, Malmqvist PA, Roos BO, Sadlej AJ, and Wolinski K (1990) Second-order perturbation theory with a CASSCF reference function. *J Phys Chem* 94:5483-5488.

24. Ghigo G, Roos BO, and Malmqvist PK (2004) A modified definition of the zeroth-order Hamiltonian in multiconfigurational perturbation theory (CASPT2). *Chem Phys Lett* 396:142-149.

25. Gozem S, Huntress M, Schapiro I, Lindh R, Granovsky AA, Angeli C, and Olivucci M (2012) Dynamic Electron Correlation Effects on the Ground State Potential Energy Surface of a Retinal Chromophore Model. *J Chem Theo Comput* 8:4069-4080.

26. Schapiro I, Ryazantsev MN, Frutos LM, Ferré N, Lindh R, and Olivucci M (2011) The ultrafast photoisomerizations of rhodopsin and bathorhodopsin are modulated by bond length alternation and HOOP driven electronic effects. *J Am Chem Soc* 133:3354-64.

27. Strambi A, Durbeej B, Ferré N, and Olivucci M (2010) Anabaena sensory rhodopsin is a light-driven unidirectional rotor. *Proc Natl Acad Sci U S A* 107:21322-6.

28. Wand A, Rozin R, Eliash T, Jung KH, Sheves M, and Ruhman S (2011) Asymmetric toggling of a natural photoswitch: ultrafast spectroscopy of Anabaena sensory rhodopsin. *J Am Chem Soc* 133:20922-32.

29. Cheminal A, Léonard J, Kim SY, Jung K-H, Kandori H, and Haacke S (2013) Steady state emission of the fluorescent intermediate of Anabaena Sensory Rhodopsin as a function of light adaptation conditions. *Chem Phys Lett* 587:75-80.

30. Kawanabe A, Furutani Y, Jung KH, and Kandori H (2007) Photochromism of Anabaena sensory rhodopsin. *J Am Chem Soc* 129:8644-9.

31. Frutos LM, Andruniów T, Santoro F, Ferré N, and Olivucci M (2007) Tracking the excited-state time evolution of the visual pigment with multiconfigurational quantum chemistry. *Proc Natl Acad Sci U S A* 104:7764-9.

32. Freedman KA, and Becker RS (1986) Comparative investigation of the photoisomerization of the protonated and unprotonated n-butylamine Schiff bases of 9-cis-, 11-cis-, 13-cis-, and all-trans-retinals. *J Am Chem Soc* 108:1245-1251.

33. Zgrablić G, Haacke S, and Chergui M (2009) Heterogeneity and relaxation dynamics of the photoexcited retinal Schiff base cation in solution. *J Phys Chem B* 113:4384-93.

34. Kandori H, Katsuta Y, Ito M, and Sasabe H (1995) Femtosecond fluorescence study of the rhodopsin chromophore in solution. *J Am Chem Soc* 117:2669-2670.

35. Granovsky AA (2014) Firefly, version 8.0.0. http://classic.chem.msu.su/gran/firefly/index.html. Available at: http://classic.chem.msu.su/gran/firefly/index.html [Accessed 2014].

36. Gozem S, Melaccio F, Lindh R, Krylov AI, Granovsky AA, Angeli C, and Olivucci M (2013) Mapping the Excited State Potential Energy Surface of a Retinal Chromophore Model with Multireference and Equation-of-Motion Coupled-Cluster Methods. *J Chem Theo Comput* 9:4495-4506.

37. Bonačić-Kouteck`y V, Köhler J, and Michl J (1984) Prediction of structural and environmental effects on the S1-S0 energy gap and jump probability in double-bond cis-trans photoisomerizion. A general rule. *Chem Phys Lett* 104:440-443.

38. Cembran A, Bernardi F, Olivucci M, and Garavelli M (2005) The retinal chromophore/chloride ion pair: structure of the photoisomerization path and interplay of charge transfer and covalent states. *Proc Natl Acad Sci U S A* 102:6255-60.

39. Salem L (1979) The sudden polarization effect and its possible role in vision. *Acc Chem Res* 12:87-92.

40. Besalú E, and Bofill JM (1998) On the automatic restricted-step rational-function-optimization method. *Theo Chem Acc* 100:265-274.

41. Gozem S, Schapiro I, Ferré N, and Olivucci M (2012) The molecular mechanism of thermal noise in rod photoreceptors. *Science* 337:1225-8.